CHEMISTRY OF MATERIALS

Article

pubs.acs.org/cm

A Bulk Boron-Based Photocatalyst for Efficient Dechlorination: $K_3B_6O_{10}Br$

Xiaoyun Fan,*[,†] Ling Zang,[‡] Min Zhang,[†] Hengshan Qiu,[†] Zhen Wang,[†] Jiao Yin,[†] Hanzhong Jia,[†] Shilie Pan,[†] and Chuanyi Wang*[,†]

[†]Laboratory of Environmental Sciences and Technology, Xinjiang Technical Institute of Physics & Chemistry, and Key Laboratory of Functional Materials and Devices for Special Environments, Chinese Academy of Sciences, Urumqi 830011, China

[‡]Department of Materials Science and Engineering, University of Utah, 122 South Central Campus Drive, Salt Lake City, Utah 84112, United States

Supporting Information

ABSTRACT: Nanoparticles of a borate nonlinear optical material, $K_3B_6O_{10}Br$ (KBB), have been fabricated and demonstrated excellent catalytic activity in UV-induced dechlorination of chlorophenols, which are typical persistent organic pollutants. The obtained dechlorination efficiency is 2 orders of magnitude higher than that of a commercial P25 TiO_2 catalyst under UV (λ > 254 nm) light irradiation. The noncentrosymmetric structure of KBB gives rise to an intrinsic large polarization effect as evidenced by Kelvin probe force microscopy, and the polarization promotes separation of photogenerated electron−hole pairs, leading to efficient cleavage of chlorophenols into small molecular fragments and dissociative Cl^- anions. This work suggests that nonlinear materials open a new window for designing efficient photocatalysts.

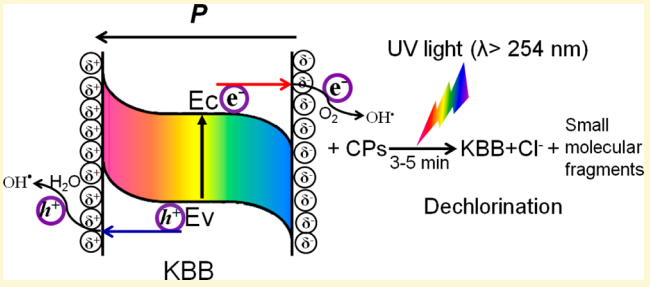

1. INTRODUCTION

Chlorophenols (CPs) represent one important class of organic pollutants,[1] for which the stable chlorine−carbon (C−Cl) bond sustains the toxicity and carcinogenicity. Cleavage of the C−Cl bond remains a critical step in the degradation process of CPs, usually occurring at the first stage of reactions.[2,3] The development of a highly effective catalyst that will allow fast dechlorination of CPs under mild reaction conditions is greatly important.[4]

Conventional processes used for removal of CPs include physical, chemical, and biological methods. Ionizing radiation such as γ-rays or electron beams has proven to be effective for degradation of a wide range of toxic organic contaminants (including CPs), though the high cost, complicated instrumentation, and safety concerns limit the wide application of these radiation technologies.[5] Zero valent (zero oxidation state) metals,[6] such as iron (Fe, zero valent iron)[7] and magnesium (Mg),[8] and bimetallic nanoparticles (Pd/Sn, Pd/Fe, and Mg-Al)[9] have been used as efficient agents for dechlorination of chlorinated compounds. The major problem with the use of these agents is the release of metals, and the formation of hydroxide or oxide layer on the particle surface during the reaction, thus significantly reducing the reactivity of the metal particles.[10] Microbial biodegradation of CPs has been widely studied.[11] However, this approach has its limitations mainly because of the low biodegradability and the toxic effects on the active biomass, which combined require specific environmental conditions and long acclimation and hydraulic retention times. Consequently, exploring new approaches to the degradation of CPs and other chlorinated contaminants based on low cost and abundant catalyst materials, while still maintaining high efficiency, remains of great interest.

Photocatalysis has been widely used for complete degradation of many organic and inorganic pollutants in water.[12] Recently, various boron-doped titanium dioxide (B-TiO_2) photocatalysts, such as B-doped TiO_2,[13] B- and Ag-codoped TiO_2,[14] B/N-TiO_2,[15] B- and N-codoped TiO_2,[16] and Ni_2O_3/$TiO_{2-x}B_x$,[17] have been developed and shown to have activity higher than that of the unmodified TiO_2. However, most of the studies focus on the chemical environment surrounding boron (e.g., B−Ti−O vs B−O−Ti) and the effect of boron doping on photocatalysis efficiency. The material fabrication techniques are generally limited regarding the control of the chemical environment of boron and the bulk phase uniformness of the crystalline structure. Room to develop new, more efficient photocatalysts, particularly those based on boron materials, remains.

As typical nonlinear optical (NLO) materials, many borate crystals exhibit high second and third nonlinear susceptibilities.[18] Because their positive and negative charges have different centers of symmetry, NLO materials belong to ferroelectric materials that have a macroscopic polarization

Received: February 18, 2014
Revised: April 17, 2014
Published: April 30, 2014

that induces the accumulation of charges at the surfaces.[19] Spontaneous polarization can be screened by free electrons and holes in the conduction and valence bands, respectively, and/or by ions or molecules adsorbed on the surface from the solution forming a Stern layer.[20] A positive charge in positive domains is screened by external and internal mechanisms.[21] The internal mechanism consists of the formation of a negatively charged region below the surface, and the external mechanism consists of the adsorption of foreign negatively charged ions or molecules at the surface. The opposite reactions take place in negative domains, and the adsorbed ions or molecules are positively charged. This charge redistribution creates an electric field in the space charge region.[22] A polarization field is compensated at equilibrium by the screening mechanisms. In this case, the photogenerated electrons can easily reach the surface and give rise to oxidation and reduction products at different locations.[23]

To the best of our knowledge, the photocatalytic property of borate crystals has never been studied, though as evidenced in this study the unique photochemistry of the NLO materials may be employed to initiate some new photoreaction pathways. Herein, we report, for the first time, on a borate NLO crystal, $K_3B_6O_{10}Br$ (KBB), which in the format of the nanoparticle suspension in water demonstrated high efficiency in dechlorination of CPs (e.g., 4-CP and 2,4-DCP) under UV (λ > 254 nm) light irradiation.

2. EXPERIMENTAL SECTION

The KBB single crystal was prepared by a top-seeded solution growth method[24] and then ground into nanoparticles.

The Brunauer–Emmett–Teller (BET) surface area was obtained from the N_2 adsorption/desorption isotherms recorded at 77 K (QUADRASORB IQ, Quantachrome Instrument Corp.).

Photocatalytic activity tests for all samples were conducted at room temperature. During the experiment, the tested photocatalyst sample was dispersed in 100 mL of a solution of CPs (50 mg/L) in a reactor and stored for 20 min while being stirred in the dark to attain adsorption equilibrium. The reactor was then illuminated by a 500 W mercury lamp with a wavelength (λ) of >254 nm. Samples were withdrawn periodically from the reactor. The percentage of residual CP solution at a selected time of irradiation is given by C/C_0, where C_0 is the concentration of the CP solution at the initial stage, i.e., right before irradiation, and C is the concentration at selected irradiation times (0, 1, 2, 3, 4, and 5 min). For comparison, parallel experiments were conducted with P-25. The concentration of each chlorophenol was measured using high-performance liquid chromatography (Ultimate 3000, Dionex) with a Supelco PAH column (4.6 mm × 250 mm). A mixture of acetonitrile, water, and acetic acid [60/39.75/0.25 (v/v/v)] was used as an effluent, and the flow rate was 1.0 mL/min. The size of the sample loop was 20 mL. The wavelength of the detector was set at 282 nm.

The photoelectrocatalytic (PEC) degradation experiments were performed in a 50 mL quartz cylinder reactor. The reactor was placed 6 cm in front of a 500 W mercury lamp (λ > 254 nm; Perfect Light Company, Beijing, China). The intensity of light at the KBB film was 0.185 W/cm^2. The photocurrents of UV light on and off studies were determined on a CHI660E electrochemical system using a standard three-electrode cell with a working electrode (20 mm × 20 mm), a platinum plate as the counter electrode, and a standard calomel electrode (SCE) as the reference electrode. The photocurrents of UV light on and off were measured at 0.065 V. Electrochemical impedance spectroscopy (EIS) measurements were taken with an electrochemical workstation (Zahner Im6ex) and conducted for the working electrode in a frequency range of 100 kHz to 0.01 Hz with ac signal amplitude of 5 mV at open circuit potential in different aqueous electrolytes. The PEC activities of the samples were all evaluated by the removal of 2,4-DCP (with an initial concentration of 50 mg/L) in a 0.1 M Na_2SO_4 solution.

Atomic force microscopy (AFM) combined with Kelvin probe force microscopy (KPFM) measurements were performed at room temperature with an Asylum Research MFP-3DTM atomic force microscope. Images were obtained in tapping mode with a scan rate of 1 Hz and an AC mode for a scan size of 1 μm × 1 μm. In the experiment, KBB nanoparticles were first dispersed in water and then sprayed on a Pt substrate. Before measurements, the sample was baked in a dry oven at 200 °C for 6 h. For the light irradiation experiment, a mercury lamp with a wavelength (λ) of >254 nm and a convex lens with a focusing spot size (d) of 1.5 cm were used to introduce focused UV light onto the measurement region between the tip of the atomic force microscope and sample.

The contents of OH$^\bullet$ radicals over samples under UV light irradiation were investigated via a photoluminescence (PL) process. Fluorescence spectra of 2-hydroxyterephthalic acid were measured on a Hitachi fluorescence spectrophotometer (F-7000). The OH$^\bullet$ radical trapping experiments were conducted using the following procedure. Terephthalic acid (TA) (16.6 mg) was first dissolved in 200 mL of a dilute NaOH solution (2×10^{-3} M), followed by addition of 100 mg of photocatalysts, and stirred for 30 min in the dark. The suspension was irradiated with a 500 W mercury lamp for 60 min. The fluorescence emission spectrum of the solution was measured every 1 min during illumination. At a defined time interval, the concentration of the solution in the system was analyzed by PL (excited by 312 nm light).

3. RESULTS AND DISCUSSION

The crystal structure of the material, as first investigated in 2006,[25] belongs to noncentrosymmetric trigonal space group $R3m$ (Figure 1a). Three [BO_4] units are joined together through corner sharing of an O atom, and another three [BO_4]

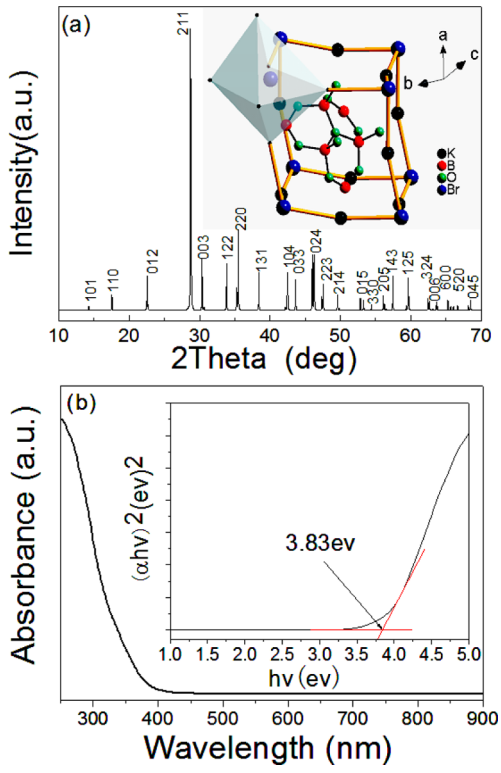

Figure 1. (a) XRD pattern of the KBB particles. The inset shows the schematic drawing of the crystal structure with the perovskite-related structure of KBB. (b) UV–vis diffusive reflectance spectrum of the KBB particles.

dx.doi.org/10.1021/cm500597e | Chem. Mater. 2014, 26, 3169–3174

units are connected with the three [BO_3] units, forming a compact hexaborate unit ([B_6O_{13}]) embedded in a K−Br network. Because the trigonal [BO_3] anionic group possesses a conjugated π orbital that can be polarized easily, it is one of the most active NLO clusters in borate crystals.[18] The crystal structure of KBB is confirmed by X-ray diffraction (XRD) analysis (Figure 1a). The particle size of the crystals was in the range of 50−400 nm as measured by scanning electron microscopy (SEM) imaging (Figure S1 of the Supporting Information). The UV−vis diffuse reflectance spectrum (Figure 1b) indicates that the KBB particles can absorb photons at wavelengths shorter than 325 nm.

As shown in Figure 2a, the photodechlorination of 2,4-DCP [under a mercury lamp (λ > 254 nm) with irradiation in the

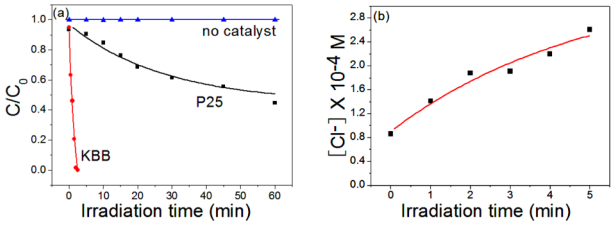

Figure 2. (a) Temporal course of photodechlorination of 2,4-DCP (50 mg L^{-1}, 100 mL) in aqueous dispersions (containing the KBB catalyst, 50 mg). The relative concentration change (C/C_0) was monitored for direct comparison of the reaction kinetics between the different catalysts used. (b) Formation of Cl^- as a function of illumination time during the photodechlorination process.

presence of KBB powders] was monitored by measuring the absorbance of DCP at 282 nm. The detailed high-performance liquid chromatography (HPLC) analysis of the aqueous solutions of 2,4-DCP under the photoreaction is supplied in Figure S2 of the Supporting Information. The concentration of 2,4-DCP decreases to almost zero within 3 min, denoting a high reaction efficiency. Approximately 70% of the total chloride content was converted into Cl^- anions after illumination for 5 min (Figure 2b). The same photodechlorination reaction was also performed on other CPs, such as 4-CP, as shown in Figure S3 of the Supporting Information. A high dechlorination efficiency was also obtained for these CPs under the same photoreaction conditions involving KBB.

For comparison, photodechlorination of 2,4-DCP was also performed in the presence of the commercial standard photocatalyst, P25 TiO_2, under the same reaction conditions that were employed for KBB. The reaction with the P25 photocatalyst was found to be significantly slower than that with KBB. The complete dechlorination of 2,4-DCP (99.8%) in the presence of KBB was achieved within only 3 min, while in the case of P25 TiO_2, it took as long as 180 min to reach the same level of degradation of 2,4-DCP (99.5%). Moreover, under simulated solar light (xenon lamp; λ > 300 nm), the photoactivity of KBB was also much higher than that of P25 TiO_2 for the degradation of 2,4-DCP (Figure S4 of the Supporting Information).

Notice that the BET surface area of KBB (0.05 m^2g^{-1}) is much smaller than that of P25 TiO_2 powder (58 m^2 g^{-1}); only 10% of the DCP was adsorbed on the KBB when the surface adsorption reached its equilibrium. Despite its much lower level of surface adsorption, KBB still demonstrated reaction kinetics ~2 orders of magnitude higher than those of P25 TiO_2 (Figure 2a), indicating the surprisingly high surface photoactivity of KBB. This high activity proved to be durable by testing the same KBB catalyst for three successive cycles of photodechlorination of 2,4-DCP (see Figure S5 of the Supporting Information).

A tentative explanation for these observations is that the KBB behaves as a crystallographic noncentrosymmetric structure, inducing a spontaneous polarization due to the displacement of the center of the positive and negative charges in a unit cell.[26] To understand the origin and magnitude of the macroscopic polarity of KBB, the local dipole moments were evaluated by a bond valence approach[27] in the individual asymmetric polyhedra as well as the alignment of these polyhedra. The calculations for trigonal [BO_3] and tetrahedral [BO_4] give values of 1.186−1.215 and 1.184−1.216 D, respectively. It is noteworthy that [B_6O_{13}] units and [KO_6Br_2] polyhedra (see Figure S6 of the Supporting Information) have a large negative charge that maintains a large dipole moment (8.96 and 8.30 D, respectively). Therefore, KBB can be easily polarized, causing a highly inductive effect[28] therein. These B−O units possess strong electron cloud overlap and prefer to attract holes and repel electrons, thus facilitating separation of the photogenerated electron−hole pairs. This in turn enhances the photocatalytic activity.

The strong photoactivity of KBB is attributed not only to the polarization from the B−O and Br−K−O bonds but also more importantly to the constructive addition of these polarizations. The intriguing feature of polarizability is that it lowers the potential energy of charged reactants and transition states regardless of whether they are positively or negatively charged.[29] The direction of the dipole moment for the KBB powder is along the [010] direction (Figure 3).

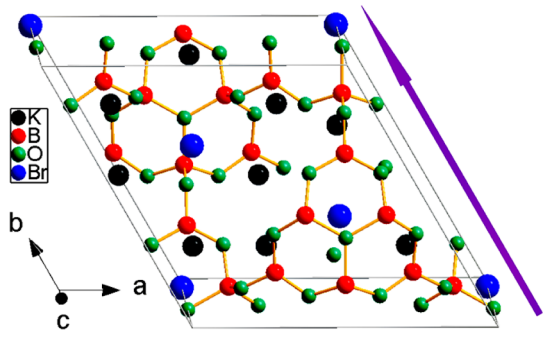

Figure 3. Ball-and-stick diagram of the KBB structure, where the purple arrows indicates the direction of the dipole moments for molecular KBB.

For a crystallographic noncentrosymmetric structure, the spontaneous polarization with directions pointing from the bulk to the surface will produce a positive charge on the surface, and the polarization pointing away from the surface to the bulk will generate a negative charge.[30] The transfer of photogenerated carriers in the KBB material is influenced by the static dipolar field, and the separated electrons and holes can move only in opposite directions for the desired reactions. In a unit cell, along the polarization vector direction (Figure 4), the field will enforce electrons to flow toward the surface to cause the reduction reaction on the surface. In the opposite direction, the field pulls the electrons away from the surface. The photogenerated holes should, obviously, exhibit behavior that is the opposite of that of electrons. Under these conditions, highly

dx.doi.org/10.1021/cm500597e | Chem. Mater. 2014, 26, 3169−3174

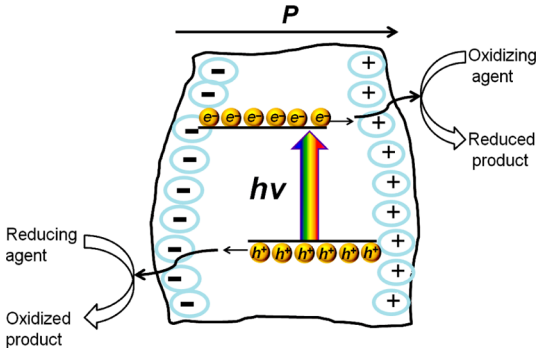

Figure 4. Schematic illustration of a noncentrosymmetric structured KBB photocatalyst.

efficient separation of the photogenerated electron−hole pairs can be achieved in the KBB materials. These hypotheses can be further supported by the measurements of the surface potential change of the KBB nanoparticles.

Surface potential measurement is a well-established approach for analyzing the illumination-induced changes in the work function of a semiconductor, in a contactless, nondestructive manner.[31] When an intrinsic built-in electric field exists in a bulk oxide induced by the spontaneous polarization, electrons photoexcited to the conduction band will migrate along the reverse direction of the electric field to one of the polar surfaces, while holes move slightly to the opposite side.[32] The charge separation process consequently leads to a change in the surface potential of both surfaces with different signs.[33] The difference in surface potential between the irradiated and nonirradiated areas can be analyzed by AFM and Kelvin probe force microscopy (KPFM).[34] In noncontact mode, the AFM and KPFM images can be derived simultaneously from one measurement. Panels a and b of Figure 5 show the morphologies of the sample before and after irradiation, respectively, and the corresponding surface potential images are shown in panels c and d of Figure 5, respectively. In panels a and b of Figure 5, no resolvable difference is observed, indicating that UV light irradiation has no influence on the morphology of the KBB nanoparticles. However, the surface potential of the whole scanned region dramatically decreases after UV irradiation (Figure 5c,d). On average, the decrease was ∼65 mV. This overall decrease in surface potential is due to the filling of electrons in the conduction band during the light excitation process. If this effect contributed equally to all faces of the nanoparticles, subtraction of one image from the other would not create any structural change in the surface potential image. However, this is not the case as shown in Figure 5e, wherein a differential surface potential image is obtained by subtracting panel d from panel c. The change in surface potential due to charge separation is reflected by the gray scale fluctuation in the image. This is direct experimental evidence of the charge separation under the intrinsic electric filed induced by the spontaneous polarization in KBB. A line scan surface potential profile is shown in Figure 5f, from which the surface potential difference between different faces due to the charge separation is deduced to be ∼10 mV. This result provides direct evidence that the electrons and holes are separated by the spontaneous polarization.

To further support the suggested polarization effect on photocatalysis described above, the photoelectrochemical (PEC) experiments,[35] including transient photocurrent response (TPC) and electrochemical impedance spectra (EIS), were employed to investigate the interface charge-transfer properties of KBB, in comparison with those of P25 TiO_2 (Figure 6).

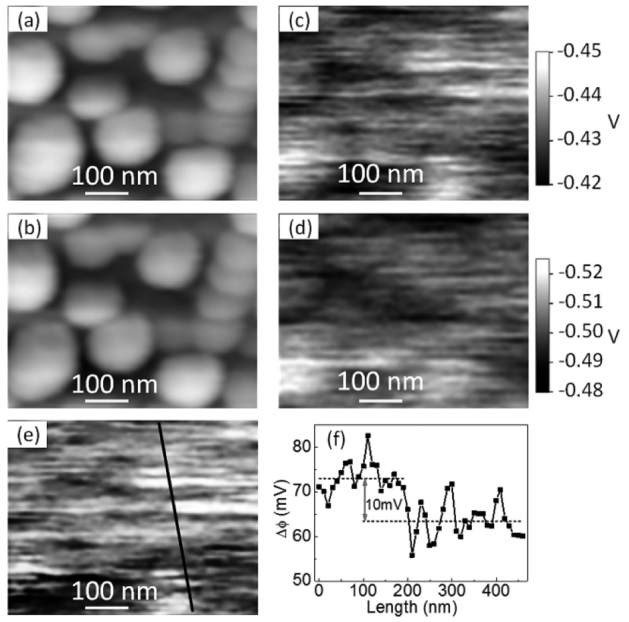

Figure 5. AFM images of KBB before (a) and after (b) UV light irradiation and corresponding surface potential images of KBB before (c) and after (d) UV light irradiation, where the bars indicate the surface potential relative to the PtIr alloy probe. (e) Differential image obtained by subtracting panel d from panel c, where the *Z* range of panel e is 30 mV. (f) Surface potential profile along the black line in panel e.

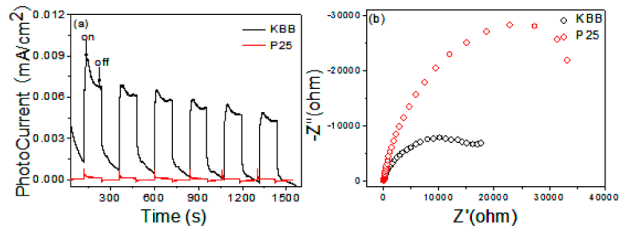

Figure 6. (a) Photocurrent spectra and (b) electrochemical impedance spectra of the KBB and P25 TiO_2.

The TPC was recorded with several on−off cycles of intermittent irradiation, and the photocurrent values obtained were normalized by the $I_{ph,in}/I_{ph,st}$ ratio, where $I_{ph,in}$ and $I_{ph,st}$ correspond to the initial and stationary photocurrents, respectively.[36] An electrode with a high $I_{ph,in}/I_{ph,st}$ ratio and $I_{ph,st}$ suggests a low rate of recombination of electrons and holes during photoreaction. Measurement of EIS can provide information about the charge transport and recombination properties of a photocatalyst, as usually presented in the form of a Nyquist plot. The smaller arc diameter in Nyquist plots indicates a lower resistance of the interfacial charge transfer. As shown in panels a and b of Figure 6, compared to P25 powder the KBB sample exhibits an ∼50 times higher $I_{ph,st}$ in TPC and a much smaller arc diameter in EIS, indicating that KBB could effectively enhance the charge separation of photogenerated electron−hole pairs as discussed above.

dx.doi.org/10.1021/cm500597e | *Chem. Mater.* 2014, 26, 3169−3174

The photodegradation mechanism of chlorophenols on KBB is similar to that on TiO_2 under UV light.[37] As shown in eqs 1−5, the holes can either react with adsorbed water (or surface-bound OH groups) to form hydroxyl radicals or directly oxidize surface organic compounds. The photogenerated electrons are scavenged by dissolved oxygen, producing superoxide ($O_2^{\bullet-}$), followed by the formation of hydroxyl radical ($OH^{\bullet}$) via a series of reactions (eqs 3 and 4).[38] $OH^{\bullet}$ radicals are believed to be the major oxidation reagent in the dechlorination and degradation of chlorophenols.[39] To confirm the formation of $OH^{\bullet}$ radicals in this system, the hydroxylation of terephthalic acid (TA) was used as an indicator of $OH^{\bullet}$ radicals, following the routine process as established previously.[40] Upon reacting with $OH^{\bullet}$, TA converts to TA-OH that emits characteristic fluorescence around 426 nm.[41] It was found in our experiment that the fluorescence intensity at 426 nm increased linearly with photoreaction time (Figure S7 of the Supporting Information), demonstrating that $OH^{\bullet}$ radicals were indeed generated in the KBB-mediated photoreactions, as summarized in eqs 1−5.

$$\mathrm{KBB} \xrightarrow{h\nu} \mathrm{KBB}\ (e^- + h^+) \quad (1)$$

$$h^+ + H_2O(\mathrm{surface}) \rightarrow OH^{\bullet}(\mathrm{surface}) + H^+ \quad (2)$$

$$e^- + O_2(\mathrm{surface}) \rightarrow O_2^{\bullet-} \quad (3)$$

$$O_2^{\bullet-} + H^+ \rightarrow HOO^{\bullet} \rightarrow OH^{\bullet} \quad (4)$$

$$OH^{\bullet} + \mathrm{CPs} \rightarrow \text{dechlorinated intermediates and products} \rightarrow Cl^- + \text{small molecular fragments} \quad (5)$$

4. CONCLUSIONS

In conclusion, we have fabricated particulate KBB, which demonstrates a photocatalytic efficiency in dechlorination of CPs superior to that of P25 TiO_2 under UV ($\lambda > 254$ nm) light irradiation. The high polarizability of KBB induces the internal electric fields at the space−charge regions, which facilitates the charge separation of photogenerated electron−hole pairs and thus enhances the photocatalytic activity. The findings are expected to open a new application scenario for nonlinear materials, via their development into novel photocatalysts.

■ ASSOCIATED CONTENT

Supporting Information

Hydroxyl radical measurement, ORTEP structures of B_6O_{13} and KO_6Br_2, HPLC, and UV absorption spectrum of the 4-CP solutions from dechlorination and repeated degradation by KBB powders. This material is available free of charge via the Internet at http://pubs.acs.org.

■ AUTHOR INFORMATION

Corresponding Authors

*E-mail: xyfan@ms.xjb.ac.cn.
*E-mail: cywan@ms.xjb.ac.cn.

Notes

The authors declare no competing financial interest.

■ ACKNOWLEDGMENTS

This work was supported by the International Science & Technology Cooperation Program of the Xinjiang Uygur Autonomous Region (Grants 20146005 and 20126017), "CAS Action Plan for the Development of Western China" (Grant KGZD-EW-502), the National Natural Science Foundation of China (Grant 21173261), the "One Hundred Talents Project Foundation Program" of the Chinese Academy of Sciences, the "Cross-Cooperation Program for Creative Research Teams" of the Chinese Academy of Sciences, and the "Western Light" Program of the Chinese Academy of Sciences (Grants XBBS 201014 and XBBS 201017).

■ REFERENCES

(1) Ahlborg, U. G.; Thunberg, T. M. *Crit. Rev. Toxicol.* **1980**, *7*, 1.
(2) Buelow, M. T.; Gellman, A. J. *J. Am. Chem. Soc.* **2001**, *123*, 1440.
(3) Czaplicka, M. *J. Hazard. Mater. B* **2006**, *134*, 45.
(4) Rong, H. P.; Cai, S. F.; Niu, Z. Q.; Li, Y. D. *ACS Catal.* **2013**, *3*, 1560.
(5) Peng, Y. X.; He, S. J.; Wang, J. L.; Gong, W. Q. *Radiat. Phys. Chem.* **2012**, *81*, 1629.
(6) Wang, C. B.; Zhang, W. X. *Environ. Sci. Technol.* **1997**, *31*, 2154.
(7) Salter-Blanc, A. J.; Tratnyek, P. G. *Environ. Sci. Technol.* **2011**, *45*, 4073.
(8) Danielw, E.; Zhang, W. X. *Environ. Sci. Technol.* **2001**, *35*, 4922.
(9) Li, T. Y.; Chen, Y. M.; Wan, P. Y.; Fan, M. H.; Yang, X. J. *J. Am. Chem. Soc.* **2010**, *132*, 2500.
(10) Boronina, T.; Klabunde, K. I. *Environ. Sci. Technol.* **1995**, *29*, 1511.
(11) Howard, P. H.; Muir, D. C. G. *Environ. Sci. Technol.* **2013**, *47*, 5259.
(12) (a) Khan, S. U. M.; Al-Shahry, M.; Ingler, W. B., Jr. *Science* **2002**, *297*, 2243. (b) Hu, C.; Hu, X.; Wang, L.; Qu, J.; Wang, A. *Environ. Sci. Technol.* **2006**, *40*, 7903. (c) Hu, C.; Peng, T.; Hu, X.; Nie, Y.; Zhou, X.; Qu, J.; He, H. *J. Am. Chem. Soc.* **2010**, *132*, 857.
(13) Chen, D. M.; Yang, D.; Wang, Q.; Jiang, Z. Y. *Ind. Eng. Chem. Res.* **2006**, *45*, 4110.
(14) Feng, N. D.; Wang, Q.; Zheng, A. M.; Zhang, Z.; Fan, J.; Liu, S. B.; Amoureux, J. P.; Deng, F. *J. Am. Chem. Soc.* **2013**, *135*, 1607.
(15) Liu, G.; Zhao, Y. N.; Sun, C. H.; Li, F.; Lu, G. Q.; Cheng, H. M. *Angew. Chem., Int. Ed.* **2008**, *47*, 4516.
(16) In, S.; Orlov, A.; Berg, R.; Garcia, F.; Pedrosa-Jimenez, S.; Tikhov, M. S.; Wright, D. S.; Lambert, R. M. *J. Am. Chem. Soc.* **2007**, *129*, 13790.
(17) Zhao, W.; Ma, W. H.; Chen, C. C.; Zhao, J. C.; Shuai, Z. G. *J. Am. Chem. Soc.* **2004**, *126*, 4782.
(18) Chen, C. T.; Lin, Z. S.; Wang, Z. Z. *Appl. Phys. B: Lasers Opt.* **2005**, *80*, 1.
(19) Stock, M.; Dunn, S. *J. Phys. Chem. C* **2012**, *116*, 20854.
(20) Cui, Y.; Briscoe, J.; Dunn, S. *Chem. Mater.* **2013**, *25*, 4215.
(21) Kalinin, S. V.; Bonnell, D. A. *Nanoscale Phenomena in Ferroelectric Thin Films*; Kluwer Academic Publications: Dordrecht, The Netherlands, 2004; pp 182−216.
(22) Dunn, S.; Jones, P. M.; Gallardo, D. E. *J. Am. Chem. Soc.* **2007**, *129*, 8724.
(23) (a) Inoue, Y.; Sate, K.; Sato, K.; Miyama, H. *J. Phys. Chem.* **1986**, *90*, 2809. (b) Li, L.; Salvador, P. A.; Rohrer, G. S. *Nanoscale* **2014**, *6*, 24. (c) Lines, M. E.; Glass, A. M. *Principles and Applications of Ferroelectrics and Related Materials*; Clarendon Press: Oxford, U.K., 2001.
(24) Fan, X. Y.; Zhang, M.; Pan, S. L.; Yang, Y.; Zhao, W. W. *Mater. Lett.* **2012**, *68*, 374.
(25) Al-Ama, G.; Belokoneva, E. L.; Stefanovich, S. Y.; Dimitrova, O. V.; Mochenova, N. N. *Crystallogr. Rep.* **2006**, *51*, 225.
(26) Goldacker, T.; Abetz, V.; Stadler, R.; Erukhimovich, I.; Leibler, L. *Nature* **1999**, *398*, 137.
(27) (a) Brown, I. D.; Altermatt, D. *Acta Crystallogr.* **1985**, *B41*, 244. (b) Brese, N. E.; O'Keeffe, M. *Acta Crystallogr.* **1991**, *B47*, 192.
(28) Ma, X. G.; Lu, B.; Li, D.; Shi, R.; Pan, C. S.; Zhu, Y. F. *J. Phys. Chem. C* **2011**, *115*, 4680.
(29) Buelow, M. T.; Gellman, A. J. *J. Am. Chem. Soc.* **2001**, *123*, 1440.
(30) Bowen, C. R.; Kim, H. A.; Weaver, P. M.; Dunn, S. *Energy Environ. Sci.* **2014**, *7*, 25.

(31) Melitz, W.; Shen, J.; Kummel, A. C.; Lee, S. *Surf. Sci. Rep.* **2011**, *66*, 1.
(32) Giocondi, J. L.; Rohrer, G. S. *Chem. Mater.* **2001**, *13*, 241.
(33) Palermo, V.; Palma, M.; Samorì, P. *Adv. Mater.* **2006**, *18*, 145.
(34) Liscio, A.; Palermo, V.; Samorì, P. *Acc. Chem. Res.* **2010**, *43*, 541.
(35) Iwashina, K.; Kudo, A. *J. Am. Chem. Soc.* **2011**, *133*, 13272.
(36) Xie, G. C.; Zhang, K.; Guo, B. D.; Liu, Q.; Fang, L.; Gong, J. R. *Adv. Mater.* **2013**, *25*, 3820.
(37) Hoffmann, M. R.; Martin, S. T.; Choi, W.; Bahnemann, D. W. *Chem. Rev.* **1995**, *95*, 69.
(38) Kisch, H. *Angew. Chem., Int. Ed.* **2013**, *52*, 812.
(39) Tao, X.; Ma, W. H.; Zhang, T. Y.; Zhao, J. C. *Angew. Chem., Int. Ed.* **2001**, *40*, 3014.
(40) Huang, H. J.; Li, D. Z.; Lin, Q.; Zhang, W. J.; Shao, Y.; Chen, Y. B.; Sun, M.; Fu, X. Z. *Environ. Sci. Technol.* **2009**, *43*, 4164.
(41) Hirakawa, T.; Nosaka, Y. *Langmuir* **2002**, *18*, 3247.